Tracing the sound horizon scale with photometric redshift surveys

E. Sánchez,[1]★ A. Carnero,[1] J. García-Bellido,[2,3] E. Gaztañaga,[4] F. de Simoni,[5] M. Crocce,[4] A. Cabré,[6] P. Fosalba[4] and D. Alonso[2]

[1]*Centro de Investigaciones Enérgeticas, Medioambientales y Tecnológicas (CIEMAT), 28040 Madrid, Spain*
[2]*Instituto de Física Teórica (UAM-CSIC), 28006 Madrid, Spain*
[3]*Département de Physique Théorique, Université de Genève, 24 quai Ernest Ansermet, CH–1211 Genève 4, Switzerland*
[4]*Institut de Ciències de l'Espai (IEEC-CSIC), 08193 Barcelona, Spain*
[5]*Observatório Nacional, 77CEP: 20921-400, Rio de Janeiro, Brazil*
[6]*Center for Particle Cosmology, University of Pennsylvania, Philadelphia, PA 19104-6322, USA*

ABSTRACT

We propose a new method for the extraction cosmological parameters using the baryon acoustic oscillation (BAO) scale as a standard ruler in deep galaxy surveys with photometric determination of redshifts. The method consists in a simple empirical parametric fit to the angular two-point correlation function $\omega(\theta)$. It is parametrized as a power law to describe the continuum and as a Gaussian to describe the BAO bump. The location of the Gaussian is used as the basis for the measurement of the sound horizon scale. This method, although simple, actually provides a robust estimation, since the inclusion of the power law and the use of the Gaussian remove the shifts which affect the local maximum. We discuss the effects of projection bias, non-linearities, redshift space distortions and photo-z precision and apply our method to a mock catalogue of the Dark Energy Survey, built upon a large N-body simulation provided by the MICE collaboration. We discuss the main systematic errors associated with our method and show that they are dominated by the photo-z uncertainty.

Key words: methods: data analysis – cosmological parameters – dark energy – large-scale structure of Universe.

1 INTRODUCTION

Primordial perturbations generate acoustic waves in the photon–baryon fluid until decoupling ($z \sim 1100$). During this time, the photons decouple from the baryons creating a high density region from the original source of perturbation, at a distance given by the sound horizon length. This high density profile shows as a peak associated with the sound horizon scale in the galaxies' spatial two-point statistics in the configuration space and as a series of oscillations in Fourier space, which can be used as a cosmological standard ruler. Recently, this feature has been applied to constrain cosmological parameters using several methods (Eisenstein et al. 2005; Hütsi 2006a,b; Padmanabhan et al. 2007; Percival et al. 2007; Okumura et al. 2008; Gaztañaga, Cabré & Hui 2009; Sánchez et al. 2009). These observations together with *Wilkinson Microwave Anisotropy Probe* 7 and Type Ia supernovae result in the concordance cosmology: a spatially flat and late-time-accelerated universe (Komatsu et al. 2010).

In order to achieve high accuracy on the cosmological parameters, several galaxy surveys estimating redshifts from photometric

data will be done, such as Dark Energy Survey (DES; The Dark Energy Survey Collaboration 2005), PanSTARRS (Kaiser, Tonry & Luppino 2000), LSST (Tyson et al. 2003) or PAU (Benítez et al. 2009). This higher accuracy will be possible, thanks to a larger volume and number of observed galaxies compared to previous spectroscopic surveys such as Sloan Digital Sky Survey (York et al. 2000) or 2dF (Colless et al. 2001), even if these photometric redshifts (photo-z) would have lower precision compared to their spectroscopic counterparts. The photo-z error depends mostly on the range of wavelengths covered by the filters in which the observations are done, the number of filters and their photometric error. As an example, the CFHTLS survey found, in the range $0.2 \leq z \leq 1.5$, a redshift error $\sigma_z \sim 0.03(1+z)$. This error was obtained with observations in the optical and the near-infrared (Ilbert et al. 2006). An error of this magnitude represents an uncertainty in the radial position of the galaxies which makes it impossible to infer the true three-dimensional (3D) clustering pattern. Therefore, the analysis of angular statistics, such as the two-point angular correlation function $\omega(\theta)$ and the angular power spectrum C_ℓ, is required for these surveys.

In this paper, a new method based on an empirical parametrization of $\omega(\theta)$ in redshift shells is proposed. The goal is to recover the angle corresponding to the baryon acoustic oscillation (BAO) scale as a

★E-mail: eusebio.sanchez@ciemat.es

function of the redshift and obtain the properties of the dark energy from its evolution.

The method is designed to be used as a standard ruler only, i.e. we do not try to use the whole shape of the correlation function or the power spectrum. The reason is that although the strict standard ruler is less sensitive to the cosmological parameters, it also seems more robust against systematic uncertainties, since the only observation to be used is the position of the BAO peak in the two-point angular correlation function and nothing else. It is unclear which measurement will be more sensitive at the end of the day, including all the systematic errors: the full description or the standard ruler (Rassat et al. 2008; Sánchez, Baugh & Angulo 2008).

The main difficulty of an approach using the position of the BAO peak as a standard ruler is the extent at which the ruler remains 'standard'. The position of the BAO peak is subject to several effects that shift its location and reduce its contrast. The most important among these is the projection offset due to the redshift bin width used to slice the data. This ultimately changes the $\omega(\theta)$ shape for wide enough binning, leaving a shoulder shape with no local maximum.

Our parametric approach is none the less able to measure the BAO scale even for wide redshift bins, and correct for the shift due to the projection effect, recovering the input cosmology. The proposed method has been tested against theoretical calculations and also applied to mock surveys from *N*-body simulations. Nevertheless, it should be useful to study BAO as a standard ruler in any photometric redshift survey.

2 ANGULAR CLUSTERING

In complete analogy to the spatial correlation function $\xi(r)$, the angular correlation function $\omega(\theta)$ is defined as the excess joint probability that two point sources (e.g. galaxies) are found in two solid angle elements, $d\Omega_1$ and $d\Omega_2$, with angular separation θ compared to a homogeneous Poisson distribution (Peebles 1980). From this definition, it is easy to find the relation between $\xi(r)$ and $\omega(\theta)$:

$$\omega(\theta) = \int_0^\infty dz_1\, \phi(z_1) \int_0^\infty dz_2\, \phi(z_2)\, \xi(r; \bar{z}) , \tag{1}$$

where $\phi(z)$ is the redshift shell selection function normalized to unity and $\bar{z} = (z_1 + z_2)/2$. This relation assumes that the time evolution of the real-space spatial correlation function is small within the redshift shell under analysis, i.e. $\xi(r; z_1) \approx \xi(r; z_2)$ (for a relation without approximations, see Matsubara, Szalay & Pope 2004). The comoving distance between two point sources for a spatially flat cosmology is (for a generalization to other spatial curvatures, see again Matsubara et al. 2004)

$$r = \sqrt{\chi(z_1)^2 + \chi(z_2)^2 - 2\chi(z_1)\chi(z_2)\cos\theta} . \tag{2}$$

The comoving radial distance $\chi(z)$, assuming a constant dark energy equation-of-state parameter w,[1] is defined as

$$\chi(z) = \frac{c}{H_0} \int_0^z \frac{dz}{\sqrt{\Omega_m(1+z)^3 + \Omega_\Lambda(1+z)^{3(1+w)}}} . \tag{3}$$

As usual, c is the speed of light, H_0 is the present-time Hubble parameter, Ω_m is the matter density parameter and $\Omega_\Lambda = (1 - \Omega_m)$ is the dark energy density parameter. With the relation between $\omega(\theta)$ and $\xi(r)$ in hand, one needs a model for the two quantities that

appear in equation (1): the spatial correlation function, including the effects of non-linearities, and the selection function $\phi(z)$ that takes into account observational effects.

The spatial correlation function is given by

$$\xi(r; z) = \int_0^\infty \frac{dk}{2\pi^2} k^2 j_0(kr) P(k; z) , \tag{4}$$

where $j_0(x)$ is the spherical Bessel function of zeroth order and $P(k)$ the power spectrum.

In linear theory, valid at large distances, $P_L(k) = b^2 D^2(z) P(k, z = 0)$, with b being a constant bias factor and $D(z) = \delta(z)/\delta(z=0)$, the growth factor of the density contrast, $\delta(z)$. Since we are only concerned with the BAO peak position and not the clustering amplitude, the bias b between luminous and dark matter will be set to unity throughout our analysis. We are assuming, then, that it does not evolve much in a redshift shell and that it is scale independent (see Section 5.4.5) as well as neglecting peak shifts in the 3D correlation of galaxies/haloes with respect to that of dark matter in front of projection effects (Sánchez, Baugh & Angulo 2008; Smith, Scoccimarro & Sheth 2008). This is a very good approximation for the scales we are dealing with, as has been measured in Cresswell & Percival (2009). A brief discussion of the systematic error that is induced by this assumption can be found in Section 5.4.

We introduce non-linear matter clustering only through a damping of the BAO wiggles in the linear spectrum, i.e. $P_L \rightarrow P_L e^{-k^2 \sigma_v^2(z)/2}$ (Bharadwaj 1996; Crocce & Scoccimarro 2006; Eisenstein, Seo & White 2007; Crocce & Scoccimarro 2008; Matsubara 2008). In doing this we discard the contribution to $\omega(\theta)$ of the additive mode-coupling term to $P(k)$, discussed in Crocce & Scoccimarro (2008) (see also Sánchez et al. 2009), which is justified because it has a negligible impact in the *angular* position of the BAO peak, in particular in comparison to projection effects (Crocce, Cabré & Gaztañaga 2010b). The quantity σ_v characterizes the scale where non-linear effects become significant. It is related to the linear power spectrum via

$$\sigma_v(z) = \left[\frac{1}{6\pi^2} \int_0^\infty dk\, P_L(k; z) \right]^{-1/2} . \tag{5}$$

In turn, the covariance matrix of $\omega(\theta)$, $\text{Cov}_{\theta\theta'} \equiv \langle \omega(\theta)\omega(\theta') \rangle$, for a given survey can be estimated by (e.g. Cabre et al. 2007, Crocce et al. 2010b)

$$\text{Cov}_{\theta\theta'}$$
$$= \sum_{l \geq 0} \frac{2(2l+1) P_l(\cos(\theta)) P_l(\cos(\theta'))}{(4\pi)^2 f_{sky}} \left[C(l) + \frac{1}{N/\Delta\Omega} \right]^2 , \tag{6}$$

where f_{sky} is the fraction of the sky covered by the survey and the ratio $N/\Delta\Omega$ is the number of galaxies per unit of solid angle in units of s rad^{-1}. What we call statistical error along this analysis is computed using this expression and applied to $\omega(\theta)$. A detailed analysis of these expressions and their applicability is given in Crocce et al. (2010).

3 THE SOUND HORIZON SCALE

The strength of the standard ruler method lies in the potential to relate rather straightforwardly the acoustic peak position in the correlation function of galaxies to the sound horizon scale at decoupling. However, these two quantities are not exactly equal (Seo & Eisenstein 2007; Sánchez et al. 2008; Padmanabhan & White 2009; Seo et al. 2008, 2010). Thus, in any standard ruler analysis it is crucial to distinguish between the following two angular scales,

---

[1] Some of the cosmological models used in this analysis are non-flat and others have non-constant w. In these cases, the full calculation has been used.
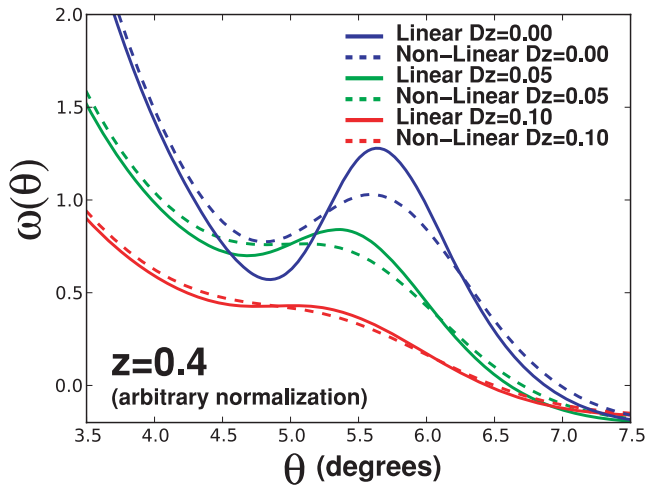
Figure 1. The impact of non-linearities and projection effects on the local maximum of the angular correlation function. The continuous line is the linear prediction and the dashed line the non-linear model from Section 2. The figure assumes a redshift bin centred at $z = 0.4$ with the upper lines (blue) corresponding to an infinitesimal shell, the middle lines (green) to a shell width of $\Delta z = 0.05$ and the lower ones (red) to $\Delta z = 0.1$. Two effects are seen. First, the position of the peak moves towards lower angles when Δz grows. Secondly, its amplitude reduces until the local maximum disappears, but a plateau survives instead. The dominant effect is the projection, while the impact of the non-linearities is much smaller.

$\theta_{\text{BAO}} \equiv r_s / \chi(z)$, the angular scale corresponding to the sound horizon at the drag epoch and θ_{p}, the location of the BAO peak in the angular correlation function, defined as the local maximum around the expected angular scale. The peak position in the linear angular correlation function θ_{p} only approaches the sound horizon scale θ_{BAO} for infinitesimal shells, but a residual difference which ranges from 1 to 2 per cent is found (Sánchez et al. 2008), depending on the cosmological parameters.

Moreover, if the survey under analysis is performed with photo-z, there will be no such thing as an infinitesimal shell, due to the uncertainty in redshift associated with the photo-z. On the other hand, the impact of the redshift space distortions on $\omega(\theta)$ is large even for large angular scales, as has been pointed out by Nock, Percival & Ross (2010), contributing also to these effects.

A large photo-z error (e.g. $\sigma_z \geq 0.03$) will require a wide redshift shell. But it is well known that this fact induces two effects, which are shown in Fig. 1. The first one is that the peak position shifts towards smaller angles and the displacement is larger for larger widths. Secondly, the amplitude of the peak gets reduced until the local maximum disappears (Loverde, Hui & Gaztañaga 2008; Simpson, Peacock & Simon 2009), and only a shoulder in $\omega(\theta)$ remains. As an order of magnitude, we have computed that for $\sigma_z = 0.01(1 + z)$ there will be a well-defined local maximum from mean redshift $z \gtrsim 0.6$ and in the case $\sigma_z = 0.03\,(1 + z)$ it will be there only for $z \gtrsim 1.3$.

These results suggest that we should measure θ_{BAO} using an alternative method to the position of the local maximum of $\omega(\theta)$. Currently, the ratio of the power spectrum to a smooth fit is used, to avoid the effect of the tilting function, which changes the peak position (Crocce & Scoccimarro 2008; Seo et al. 2008, 2010; Smith et al. 2008). Here we present an alternative method based on the angular correlation function. This will be the subject of the subsequent sections.

4 METHOD TO RECOVER θ_{BAO}

Trying to overcome the problems induced by the photo-z, we propose a new method based on an empirical parametrization of $\omega(\theta)$, which can be used even when there is no local maximum. The most important points of the method, the parametrization of $\omega(\theta)$ and the correction for the projection effect due to the width of the redshift bin, are explained in detail in Sections 4.1 and 4.2, respectively. The full recipe to obtain the BAO scale as a function of redshift is as follows.

(i) Divide the full galaxy sample into redshift bins.

(ii) Compute the angular two-point correlation function in each redshift bin.

(iii) Parametrize the correlation function using the expression

$$\omega(\theta) = A + B\theta^\gamma + Ce^{-(\theta - \theta_{\text{FIT}})^2/2\sigma^2} \tag{7}$$

and perform a fit to $\omega(\theta)$ with free parameters $A, B, C, \gamma, \theta_{\text{FIT}}$ and σ.

(iv) The BAO scale is estimated using the parameter θ_{FIT} and correcting it for the projection effect (see equation 8). The BAO scale as a function of the redshift is the only parameter needed to apply the standard ruler method. The cosmological interpretation of the other parameters is limited, since this is an empirical description, valid only in a neighbourhood of the BAO peak, as is described in Section 4.1.

(v) Fit cosmological parameters to the evolution of the corrected θ_{BAO} with z.

4.1 Parametrization of $\omega(\theta)$

The correlation function $\omega(\theta)$ is parametrized as in equation (7). A power law is used to describe the shape of the correlation function before and after the peak and a Gaussian to describe the BAO feature. The mean of the Gaussian is used to locate the BAO scale. The parameter A takes into account the fact that the correlation function can go to negative values after the BAO peak. The parameters B and C describe the relative weight of the two terms of the parametrization. The parameter γ is the index of the power law, while θ_{FIT} and σ are the mean and the width of the Gaussian, respectively.

We have tested the goodness of this parametrization in a redshift interval which ranges from 0.2 to 1.4, for a wide range of widths of the redshift bins (from 0 to 0.2) and for 14 cosmological models, which are listed in Table 1. The parametrization is good within 1 per cent, i.e. the fit is good (the value of χ^2/ndof ranges from 0.98 to 1.01 and the probabilities of the fit from 0.6 to 0.9) when the error in each point of the correlation function is ~ 1 per cent for all bin widths and cosmological models. This precision is much better than that expected in any realistic redshift survey, since it is much smaller than the cosmic variance. Several examples of the parametrization can be seen in Fig. 2. Other functional forms have been tested, but all of them are more complex and show no improvements in the description of the data.

There is a region of stability to choose the starting and end points of the fit, which will be described in more detail in Section 5.4.1. This region cannot be made arbitrarily large, since the description cannot be good for very low angles, due to non-linearities and changes in the power-law index, nor for very large angles, since the correlation function changes its slope after the BAO peak.

Table 1. Summary of the 14 cosmological models used to test the method. Where empty, the fiducial values (first line) are assumed.

h	Ω_M	Ω_b	Ω_k	w_0	w_a	n_s
0.70	0.25	0.044	0.00	−1.00	0.0	0.95
0.68						
0.72						
	0.20					
	0.30					
		0.040				
		0.048				
			+0.01			
			−0.01			
				−0.90		
				−1.10		
					−0.1	
					+0.1	
						1.00

4.2 Correcting for projection effects

The projection offset discussed in Section 3 is also present for the parametrization method. If we want to extract cosmology from this measurement, it is necessary to correct the fitted θ_{FIT} for the projection effect to recover θ_{BAO}:

$$\theta_{BAO} = \alpha\theta_{FIT},\tag{8}$$

where α could in principle be a function of redshift, bin width and cosmology. However, if we want to do this correction in an unbiased way, it must be cosmology independent. We have tested the method for the 14 different cosmologies summarized in Table 1 and for different redshift bin widths.

For each of the 14 considered models, each of the considered redshifts and each of the considered bin widths, we compute the angular correlation function. We use equation (1) and include non-linearities (see Section 2). The calculation also includes the effect of the galaxy distribution with the redshift, as described in Section 5.2. The redshift ranges from 0.2 to 1.4 and the bin width from 0 to 0.2, as has been previously stated. We then apply the fitting method to

obtain the position of the BAO peak. Two main results are obtained as follows.

(i) The shift of θ_{FIT} with respect to θ_{BAO} has a universal shape, independent of the cosmology. Thus the correction function α depends only on redshift and bin width, but not on the cosmological model, i.e. $\alpha = \alpha(z, \Delta z)$, within a precision of <1 per cent.

(ii) After applying this universal shift, the recovered BAO scale agrees with the true value for all cosmologies to a precision of ≤0.75 per cent. In particular, for infinitesimal bin widths, the method is able to compensate the displacement of the BAO bump due to the tilting function, correcting the 2 per cent difference which has been observed in Sánchez et al. (2008).

These two results are presented in Fig. 3, where we plot the evolution of the shift, taking the angular scale corresponding to the sound horizon scale as the reference, for five different redshifts, for several bin widths and for the 14 cosmological models. The spread of the results is constant with the redshift bin width and comes from a possible residual dependence on the cosmology together with the intrinsic limitations of the method (see Section 5.3 on systematic errors). The average value of this shift is the correction applied to the fitted θ_{FIT}. After this correction, the true value for the BAO scale is recovered for any bin width and cosmology. Note that the absolute value of the projection effect changes with the cosmological model, since both the BAO position and the radial distance change. However, the relative effect is cosmology independent, as shown in Fig. 3.

As has already been noted (Simpson et al. 2009), the projection effect is much more pronounced at low redshift. This must be taken into account to choose the optimum size of the redshift bins. The correction must be kept as small as possible, given the limitations imposed by the photo-z precision, to introduce small systematic uncertainties. We are using a Gaussian form for the photo-z uncertainty, because if the requirements on photo-z measurement for a survey like DES are fulfilled, the effects of a possible non-Gaussianity will be small. If this is not the case, the evaluation of the true width of the bin must be refined. This is another reason to maintain the correction small. The effect of non-Gaussian photo-z errors is twofold. First, it increases the final error due to the
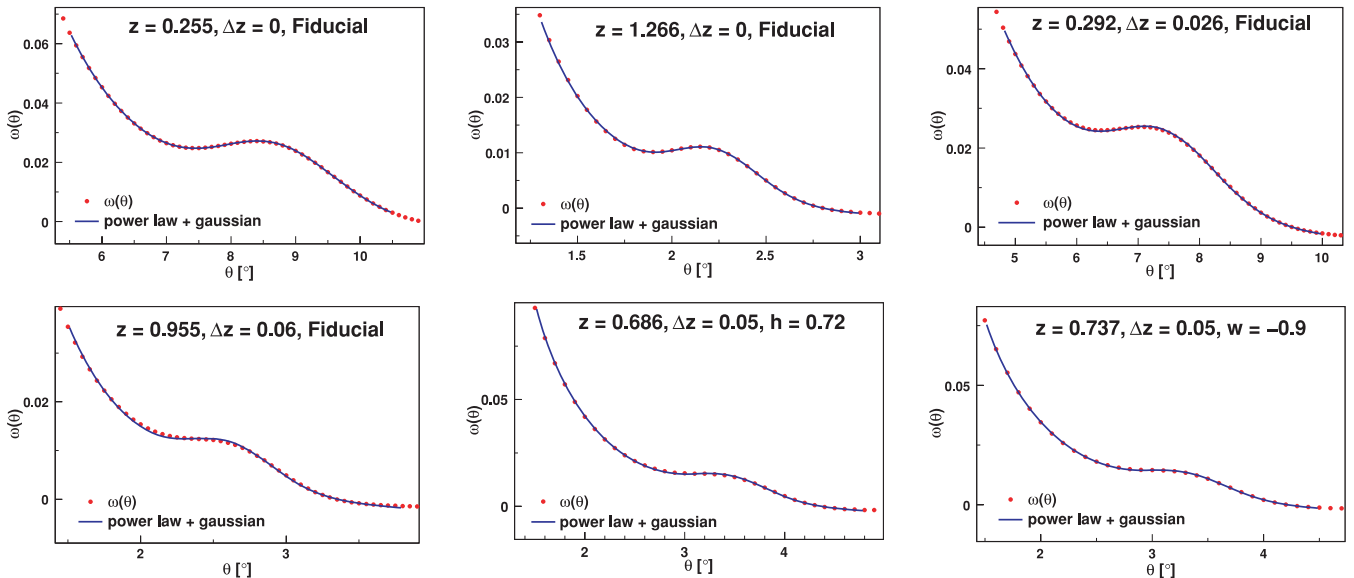
**Figure 2.** Goodness of the parametrization for several redshifts, several bin widths and several cosmologies.
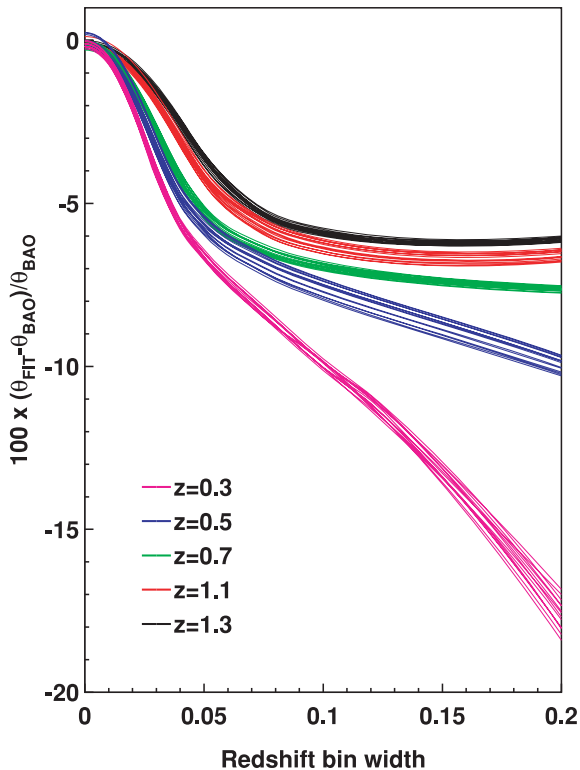
Figure 3. Evolution of the shift of the measured θ_{FIT} with the width of the redshift bin for the 14 cosmological models considered in this work. The sound horizon scale θ_{BAO} for each cosmological model is taken as the reference. Two results are obtained. First, the correct sound horizon scale is recovered for any cosmological model within 0.75 per cent for infinitesimal redshift shells. Secondly, the shape of the shift is universal, and the spread is constant with the redshift bin width. Note that the dispersion between models is much smaller (≤ 1 per cent) than the shift due to increasing bin width. At low redshifts, $z < 0.3$, the shift can be ~ 15 per cent for $\Delta z \geq 0.1$, while at high redshifts, $z > 0.5$, the shift saturates at around 7 per cent.

influence of photo-z in the determination of θ_{BAO}. Secondly, it increases the correlation between redshift bins. A small fraction of the galaxy sample (of the order of 1 per cent) with large photo-z errors (two to three times larger than the nominal value) could translate into an increase of ~ 10 per cent in the final error in θ_{BAO}.

Note that the BAO scale is recovered for both linear and non-linear theory for infinitesimal bin width. This can be seen in Fig. 4, where the residual of the fit with respect to the theoretical θ_{BAO} as a function of redshift is shown for the fiducial cosmological model. The recovered values are well inside the 0.75 per cent precision that we quote as systematic error, represented by the dotted lines. This happens for all the cosmological models, showing that the method is robust and able to recover the theoretical BAO scale.

4.3 Redshift space distortions

There are other effects which are important in order to have under control the parametric description of the angular correlation function. In particular, redshift space distortions must be taken into account in the analysis of the BAO scale, since they result in an anisotropic correlation function. We need to replace $\xi(r)$ in equation (1) by $\xi(\sigma, \pi)$ with $\pi = \chi_2 - \chi_1$, the radial separation, and $\sigma^2 = 2\chi_1\chi_2(1 - \cos\theta)$, the perpendicular separation. Galaxy pairs separated by large radial distances infall into each other which means that they are measured as contributing to bins of smaller
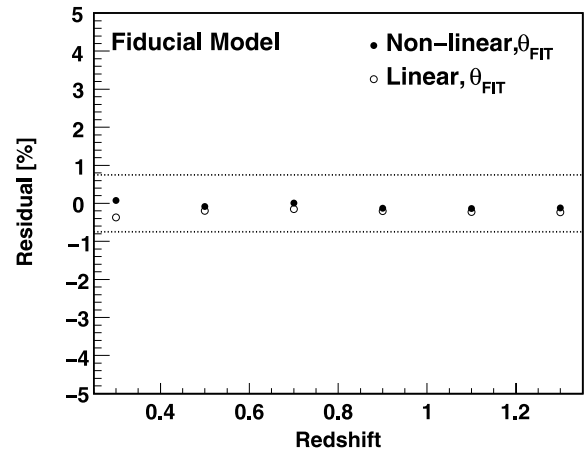

Figure 4. Residual of the result of the parametric fit θ_{FIT} with respect to the theoretical value of the BAO scale as a function of redshift for the fiducial model. The open dots show the results obtained from the fit to the linear correlation functions and the solid dots show the results on the non-linear correlation functions. In both cases the theoretical values are recovered, well inside the quoted systematic error of 0.75 per cent, shown by the dotted lines.

radial separation in redshift space than in real (or true) space. This results in larger correlations (more pairs) at intermediate scales ($\pi < 20$ Mpc h^{-1}) and lower correlations at larger separations. The redshift space correlation becomes negative for $\pi > 40$ Mpc h^{-1} while the real space correlation remains positive until $\pi > 130$ Mpc h^{-1} (see fig. A1 in Gaztañaga et al. 2009). Recall from equation (1) how the angular correlation is just a mean over the radial distance within the corresponding redshift bin. This means that for narrow redshift bins (of width comparable to $\pi \simeq 100$ Mpc h^{-1}), the resulting angular correlation can be quite different in real and redshift space (Fisher et al. 1995; Padmanabhan et al. 2007; Nock et al. 2010). As the total number of pairs is conserved, the integral over all separations is the same in real and redshift space, so that one expects to find the same angular correlation only for broad redshift bins, where the contribution of the boundary to the integral is negligible.

The resulting predictions for redshift space agree very well with MICE simulations (more details can be found in Crocce et al. 2010b). Fig. 5 shows some examples of this redshift space modelling for linear theory for two of the redshift bins used in the analysis presented above. Symbols (with 2 per cent nominal errors) correspond to the linear model predictions when we include the redshift space distortions as well as photo-z distortions. Note how both redshift space and photo-z distortions change quite dramatically the amplitude of the resulting angular correlation.

The lines in Fig. 5 show the results of a fit of our parametrization (in equation 7) to these new predictions. The corresponding fit values of θ_{FIT} are shown in the label. As expected, there is a small but systematic shift of θ_{FIT} to smaller angles in the case of photo-z distortions. This is because the effective redshift bin is wider due to the photo-z errors. This effect is taken into account by the correction shown in Fig. 3 (once we use the equivalent width of the true redshift distribution). Crocce et al. (2010b) shows that the model we are using to predict the errors also works in redshift space.

As can be seen in Fig. 5, the parametrization absorbs very well the effects of redshift space distortions and the value recovered for θ_{FIT} agrees well in real and redshift space despite the large difference in amplitude. This is not too surprising as we have already shown
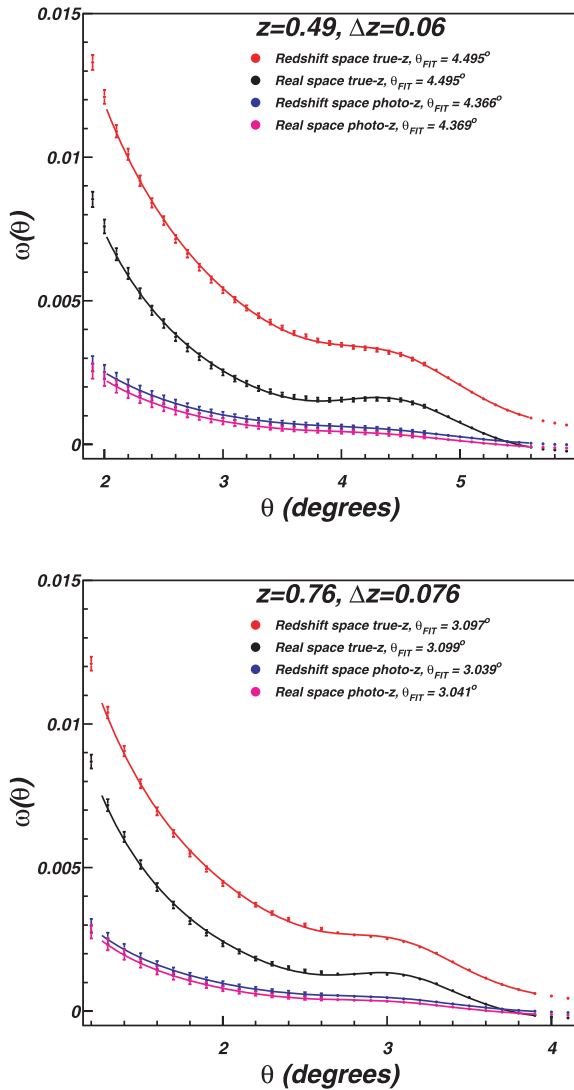
Figure 5. Effect of z-distortions and photo-z. Points (with nominal 2 per cent errors) show the linear theory prediction, while lines correspond to a fit to our parametrization in equation (7). Labels indicate the corresponding values of θ_{FIT} in each case.

above that this parametrization works for different cosmological models, different redshifts and also different redshift widths.

5 APPLICATION TO THE DARK ENERGY SURVEY

5.1 The Dark Energy Survey

DES[2] is a next-generation sky survey aimed directly at understanding the nature of the dark energy. It will use 30 per cent of the available time on the Blanco telescope at Cerro Tololo Inter-American Observatory, for 5 yr. The survey is designed to produce photometric redshifts in the range $0.2 < z < 1.4$ and will cover 5000 deg^2 in the Southern hemisphere. The filters to be used are g, r, i, z, Y.

DES has been designed to exploit mainly four methods in order to study the dark energy. These methods are the galaxy cluster
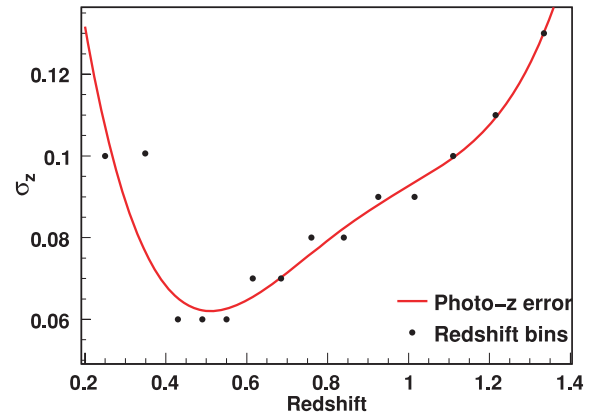
Figure 6. Photo-z precision used in this analysis (continuous line), as compared to used bin positions and widths (dots).

counting and spatial distribution of galaxy clusters, the shifting of the galaxy spatial angular power spectra with redshift, weak gravitational lensing measurements on several redshift shells and distances to $\sim$2000 supernovae. Using these techniques, a 5–15 per cent precision measurement in the equation-of-state parameter w from each of our methods and a 30 per cent measurement in the variation of w with time are expected. Combined, they provide both stronger constraints and a check on systematic errors.

5.2 N-body simulation features

We have developed and tested our method to recover the angular scale of the sound horizon using a large N-body simulation capable of reproducing the geometry (e.g. area, density and depth) and specifications of DES.[3]

The simulated data were provided by the MICE project team and consisted of a distribution of dark matter particles (galaxies henceforth) with the cosmological parameters fixed to the fiducial model of Table 1. The radial profile matches the DES expectation

$$\mathrm{d}N/\mathrm{d}z \propto (z/0.5)^2 \exp{-(z/0.5)^{1.5}}; \tag{9}$$

the simulation covers one-eighth of sky ($\sim$5000 deg^2) in the redshift range $0.2 < z < 1.4$, containing 50 million galaxies. All these numbers roughly match the DES expectations for the main galaxies. These data was obtained from the comoving output at $z = 0$ of one of the largest N-body simulations completed to date, with comoving size $L_{\mathrm{box}} = 3072\,h^{-1}$ Mpc and more than 8×10^9 particles ($m_{\mathrm{p}} = 2.3 \times 10^{11}\,h^{-1}\,\mathrm{M}_\odot$). More details about this run can be found in Fosalba et al. (2008) and Crocce et al. (2010a).

The precision in the determination of the redshift for galaxies which have been used in this analysis is shown in Fig. 6. This is the typical precision that is obtained using the current photo-z codes for DES (Banerji et al. 2008). This photo-z has been introduced into the simulation, to produce a catalogue of galaxies similar to that expected in DES, where the proposed procedure to recover θ_{BAO} has been applied. The photo-z has been introduced by scattering each individual redshift according to the Gaussian representing the photo-z error of Fig. 6. The redshift bin widths have been chosen as a compromise between statistics, expected precision in the photo-z determination and shift of the BAO peak due to projection effect. Then, the redshift bins used in this analysis follow the expected precision in the photo-z measurement, being wider for low and high

redshifts and narrower for mid-redshift. The analysis is performed in the full redshift range, from $z = 0.2$ to 1.4. With this prescription we have 14 bins, represented also as dots in Fig. 6. The position of the dot in the horizontal axis represents the bin centre, and the position in the vertical axis represents the bin width, which has been chosen to be close to the expected 1σ error in photo-z measurement. Much wider bins make the sensitivity too small due to projection effect (the amplitude of the correlation function becomes very small and the shift of the peak becomes very large), while much narrower bins make the correlations between redshift bins too large, complicating the analysis and also diminishing the sensitivity.

5.3 Results

In order to numerically estimate the angular correlation function in a given redshift bin, we have used the Landy–Szalay estimator (Landy & Szalay 1993). The random catalogues contain as many galaxies as the simulation, since the shot noise error is negligible, given the size of the sample.

The resulting correlation functions together with their parametrizations are presented in Fig. 7. The statistical error in θ_{FIT} is given as the error in the fit coming from the error in the correlation function, as explained in Section 2, and taking into account the photo-z effect, as described in equation (12).

The recovered values of θ_{BAO} after applying the correction of equation (8) can be seen in Fig. 8 (top panel) as a function of the redshift. The correction is applied after evaluating the true width of the redshift bin, using $\Delta z_{\text{true}} = \sqrt{2\pi}\,\Delta z_{\text{photo}}$, which corresponds to the width of a top-hat bin in true-z which gives the same amplitude in $\omega(\theta)$ than the chosen photo-z bin. The points also include the systematic errors, described in Section 5.4. The MICE cosmology is shown as a solid line and the best-fitting cosmology as a dashed line. To compare, the same analysis has been applied to the true redshifts catalogue (i.e. without photo-z). The corresponding result is presented in the bottom panel of Fig. 8, together with the photo-z. The results obtained using the true redshift are closer to the MICE cosmology, as expected. For true redshifts, the bin width is not corrected, and the systematic errors do not include any photo-z contribution. The evolution of the error on the measured BAO scale as a function of redshift is shown in Fig. 9. The statistical error (solid dots) dominates at low redshift ($z \leq 0.5$), while the photometric redshift error (solid triangles) becomes dominant for large redshifts ($z \geq 0.5$). The other systematic errors (open dots) are always subdominant. The large values for the statistical error at redshifts 0.685 and 1.015 are due to the smaller significance of the peak detection for those redshift bins, which makes the precise location more difficult, increasing the error.

The true cosmology is recovered after applying the analysis method, both for the photo-z results and for the true-z results. The photo-z result is shown in Fig. 10, where the MICE cosmology is inside the 1σ contours. These contours have been obtained fitting the cosmology to the results presented in Fig. 8 (top panel), with free parameters Ω_{M} and w, and fixing all the other parameters to their MICE values.

In order to perform this fit, we need to take into account the correlation between bins induced by photo-z. To do this, we compute the migration matrix r_{ij}, given by the probability that a given galaxy at bin i is measured at bin j due to the photo-z error. Once the migration matrix is computed (just counting the number of galaxies that migrate from bin i to bin j in the simulation), the calculation of

the covariance matrix C_{ij} is straightforward. Since

$$N_i^{\text{O}} = \sum_{j=1}^{N_{\text{bins}}} r_{ij} N_j^{\text{T}}, \tag{10}$$

where N_i^{O} is the number of observed galaxies in bin i, r_{ij} is the migration matrix and N_j^{T} is the true number of galaxies in bin j, the observed and true correlation functions are related by (Benjamin et al. 2010),

$$w_i^{\text{O}}(\theta) = \sum_{k=1}^{N_{\text{bins}}} r_{ik}^2 \frac{\left(N_k^{\text{T}}\right)^2}{\left(N_i^{\text{O}}\right)^2} w_k^{\text{T}}(\theta), \tag{11}$$

where $w_i^{\text{O}}(\theta)$ is the observed correlation function in bin i at scale θ and $w_i^{\text{T}}(\theta)$ is the true correlation function in bin i at scale θ, given by equation (1). Then, the covariance for the correlation functions can be written as

$$C_{ij} = \left\langle \Delta w_i^{\text{O}}(\theta)\Delta w_j^{\text{O}}(\theta') \right\rangle = \sum_{k=1}^{N_{\text{bins}}} \left(r_{ik}^2 r_{jk}^2\right) \frac{\left(N_k^{\text{T}}\right)^4}{\left(N_i^{\text{O}}\right)^2 \left(N_j^{\text{O}}\right)^2} \text{Cov}_{\theta\theta'}, \tag{12}$$

where $\text{Cov}_{\theta\theta'}$ is given in equation (6). This expression neglects the intrinsic correlations between bins. Whether this is a good approximation depends mainly on the bin widths. In our case, adjacent bin centres are separated by more than 200 Mpc h^{-1}, and we find that the intrinsic cross-correlations can be safely ignored. Thus, with photo-z errors, the observed correlation functions and covariances are given by equations (11) and (12), respectively, rather than equations (1) and (6).

The resulting correlation coefficients, computed from C_{ij}, for redshift bins are depicted in Fig. 11. The induced correlation extends to three bins. This correlation matrix is converted to the covariance of θ_{BAO} angles, $\widehat{C}_{ij}$, including the corresponding errors.

Therefore, we use the $\widehat{C}_{ij}$ to compute the χ^2 for the fit in the usual way:

$$\chi^2(\Omega_{\text{M}}, w) = \sum_{i,j}^{N_{\text{bins}}} \left(\widehat{\theta}_{\text{BAO}}^i - \theta_{\text{BAO}}^i\right) \widehat{C}_{ij}^{-1} \left(\widehat{\theta}_{\text{BAO}}^j - \theta_{\text{BAO}}^j\right), \tag{13}$$

where θ_{BAO}^i is the angular scale corresponding to the sound horizon for cosmological parameters Ω_{M}, w at the redshift of bin i and $\widehat{\theta}_{\text{BAO}}^i = \alpha\theta_{\text{FIT}}$ is the measured angle in bin i. All results include the systematic errors in the measurements of $\widehat{\theta}_{\text{BAO}}$, described in more detail in the next section. The statistical error is correlated using the computed covariance matrix. Some of the systematic errors (coming from photo-z and redshift space distortions) are also correlated, while the others are uncorrelated and are just added in quadrature to the diagonal of the covariance matrix. All these numbers match the DES requirements. The total area of the survey, together with the magnitude limits, which fix the galaxy density, contributes to the errors on $\omega(\theta)$. Moreover, the photo-z requirements fix the level of correlation among redshift bins.

If we restrict to a one-dimensional analysis and fix $\Omega_{\text{M}} = 0.25$, then we obtain for the equation of state of the dark energy $w = -1.05 \pm 0.14$. The precision on this result depends on the photo-z error, which is the dominant source of systematic uncertainties. If the photo-z error is decreased, the precision in w correspondingly improves. For a more optimistic estimation of $\Delta z \sim 0.03\,(1 + z)$, it becomes $\Delta w \sim 0.10$. These measurements are in good agreement with the Fisher matrix forecasts for BAO in DES (The Dark Energy Survey Collaboration 2005).
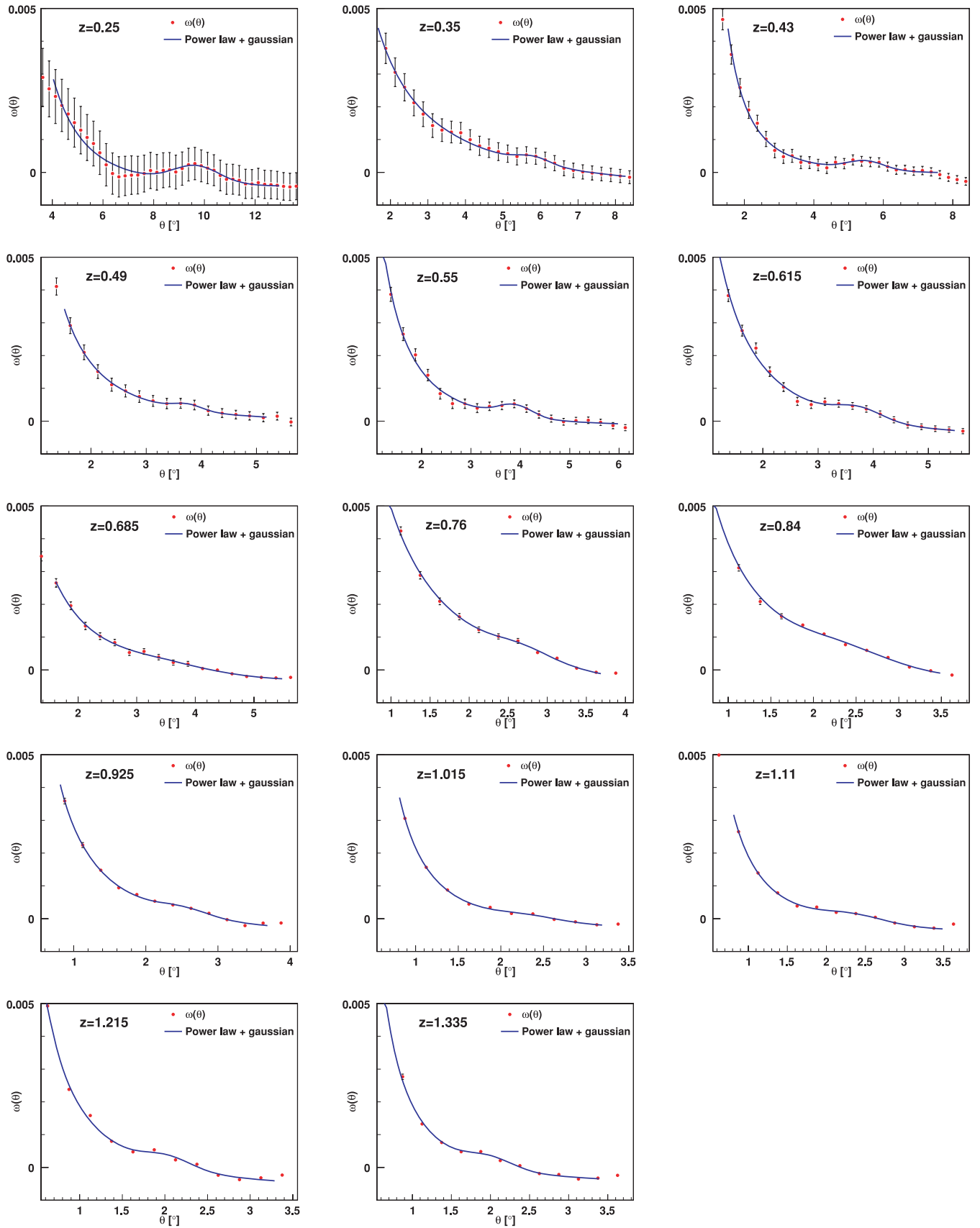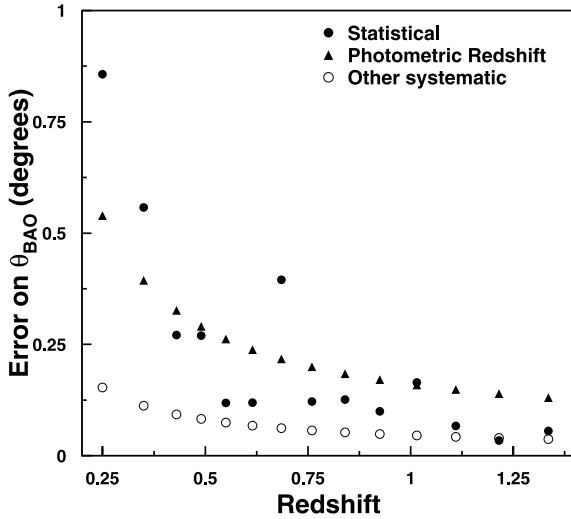
Figure 7. Correlation functions for MICE simulation, including photo-z effects. The errors are computed using equation (12).
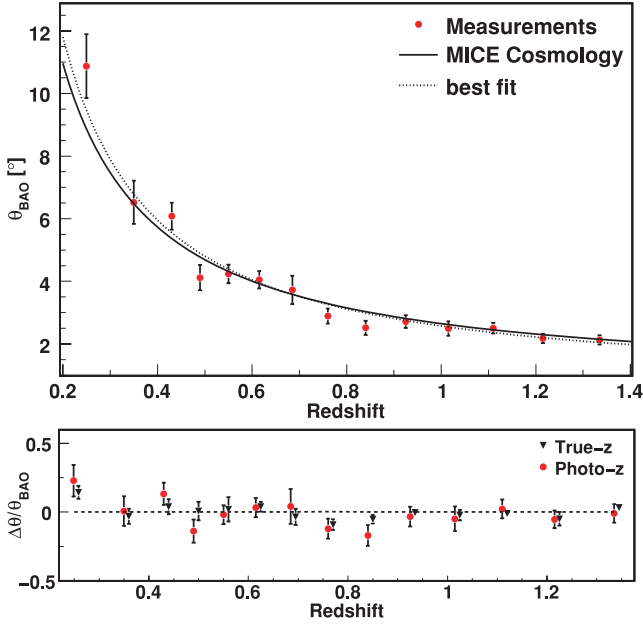
Figure 8. Evolution of the measured θ_{BAO} with the redshift (top panel). Comparison of the results obtained using photo-z and the true-z (bottom panel). The true-z results are closer to the MICE cosmology, as expected.


Figure 9. Error on the measured BAO scale as a function of redshift. The statistical error (solid dots) dominates at low redshift ($z \leq 0.5$), while the photometric redshift error (solid triangles) is dominant for large redshifts ($z \geq 0.5$). The other systematic errors (open dots) are always subdominant. The large values for the statistical error at redshifts 0.685 and 1.015 are due to the smaller significance of the peak detection for those redshift bins that make the precise location more difficult and increase the error.
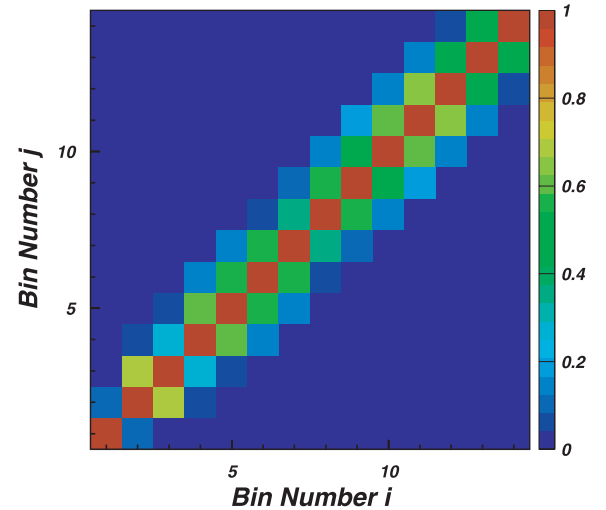
5.4 Systematic errors

We have identified several sources of systematic errors for this methodology:

(i) uncertainties in the fitting procedure (method error);
(ii) residual errors due to the correction in θ_{FIT} coming from a possible residual dependence on the cosmological model (cosmology independence);
(iii) uncertainties in the theory coming from the implementation of non-linearities (modelling error);
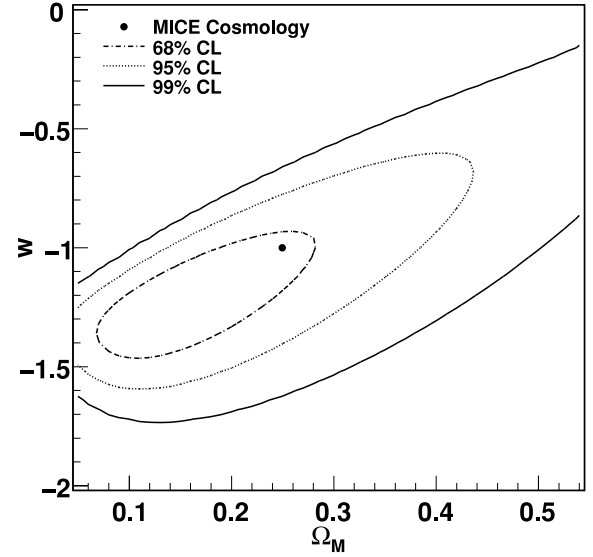
Figure 10. Allowed region for the cosmological parameters at 68 (dash–dotted line), 95 (dashed line) and 99 (solid line) per cent confidence limit. The true cosmology, given by the dot, is recovered within 1σ.


Figure 11. Correlation matrix for redshift bins. The correlation extends to three bins and is taken into account in the fit of the cosmological parameters.

Table 2. Estimation of various systematic errors. Some of them are correlated between redshift bins (photo-z and z-distortion errors). The others are not.

Systematic error	$\Delta\theta_{BAO}$ (per cent)	Correlated between bins
Parametrization	1.0	No
Photometric redshift	5.0	Yes
Redshift space distortions	1.0	Yes
Theory	1.0	No
Projection effect	1.0	No

(iv) effects of the redshift space distortions on the BAO scale (z-distortions' error);
(v) uncertainty in the redshift determination (photo-z error).

A brief quantitative summary of these effects is given in Table 2, which follows from the different analysis discussed below.
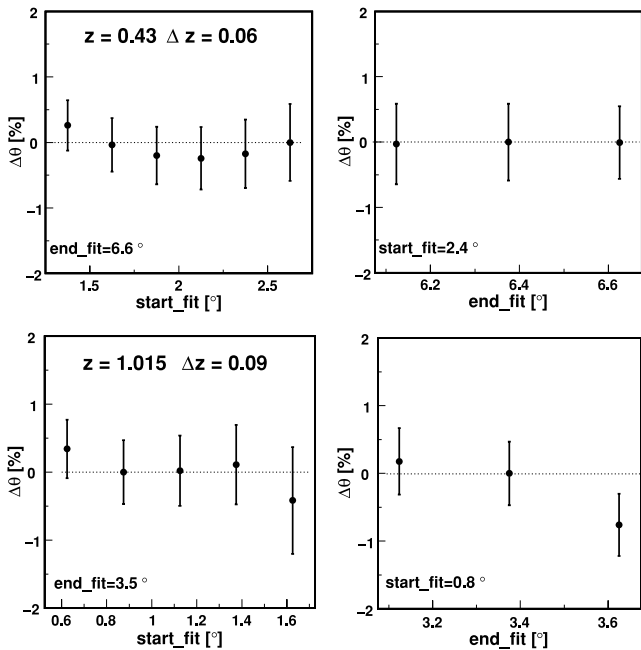
Figure 12. θ_{BAO} dispersion as a function of the starting and end points of the fitted region. Only two bins are shown, where the maximum of the effect is observed, at redshifts 0.43 (top panels) and 1.015 (bottom panels). All the bins behave in a very similar way, but with smaller variations. The observed variation in the results is slightly smaller than 1 per cent, and a conservative 1 per cent systematic error is associated with the fit method.

5.4.1 Method error

To compute the systematic error associated with the parametrization method, we have done some further analysis on theoretical angular correlation functions with the same bin widths and central redshifts as those used in the analysis of the MICE simulation. The error associated with the method comes from the possible influence in the obtained θ_{FIT} of the range of angles used to perform the fit. To evaluate the error, we have varied this range for all the 14 z-bins we have and performed the fit for each range.

In order to decide the range to be fitted, we have to choose a starting point at angles smaller than the BAO peak and an end point after the peak. By varying these two angles, we can study how much the result varies with this decision. Results can be seen in Fig. 12, where the obtained θ_{FIT} is shown for different starting points and end points of the fit, for low and high redshifts. These results show the bins where the maximum differences are observed. In all cases, the uncertainty is always of the order of, but slightly below, 1 per cent. We have conservatively assigned a 1 per cent systematic error associated with the method, since this error is subdominant.

5.4.2 Cosmology independence

The dispersion of all the cosmological models around a common value for the projection effect correction is small, ≤ 1 per cent, as can be seen in Fig. 3. This dispersion propagates directly to the corrected θ_{FIT} as a source of uncertainty. Conservatively, we have assigned a systematic error of 1 per cent associated with the independence of the cosmology.

5.4.3 Modelling error

Also, the error due to the uncertainty in the theory (non-linearities at the scale of the BAO peak) has been computed obtaining a global error of 1 per cent, estimated in a conservative way as the difference between the θ_{FIT} measured using linear and non-linear $\omega(\theta)$, for the same redshift bins of the analysis. The difference for infinitesimal bins is presented in Fig. 4.

5.4.4 Photo-z error

To compute the systematic error associated with photo-z measurement, we have analysed the simulation using the true redshifts in the same way as we do for the photo-z. We can estimate the deviation in θ_{FIT} due to photo-z errors computing the difference between the result obtained using the catalogue with true-z and that obtained using the catalogue with photo-z. In Fig. 13 (top panel), we can see the distribution of these differences. Photo-z uncertainties do not introduce a significant bias, but they do introduce a dispersion around the central value. This dispersion is around 5 per cent, which we assign as the systematic error coming from the photometric error. We are assuming here that this error is redshift independent, which, given the scope of the current analysis, is reasonable, as shown in Fig. 13 (bottom panel). The differences between the results of the analysis using photo-z and true-z are shown as a function of the redshift, and there is no indication of any redshift dependence. This estimation could be further refined by using many simulations and repeating this study as many times as simulations we use for each redshift bin. This is beyond the scope of this work, where we can only indicate the order of magnitude of the systematic errors, but should be done for a real survey, since this will be the dominant source of systematic uncertainty.
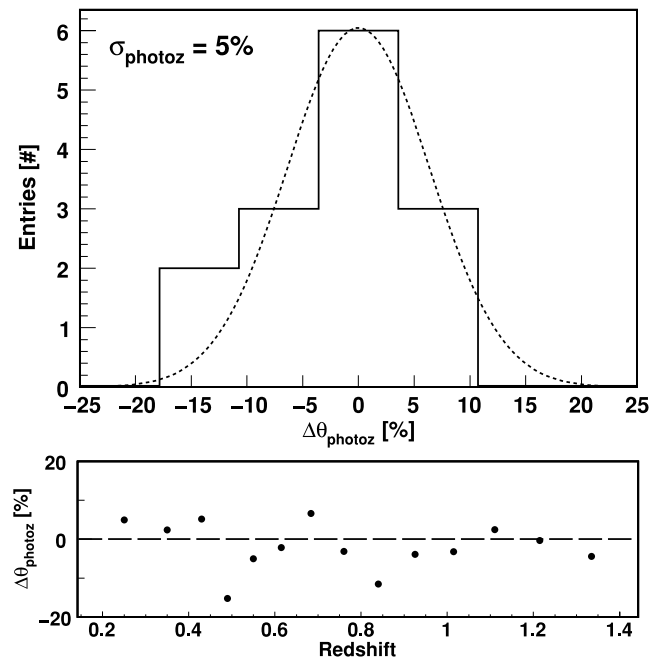
Figure 13. Cumulated difference between the measured θ_{FIT} in the photo-z catalogue and the true-z catalogue for the 14 bins of the analysis (top panel). The dispersion is 5 per cent, which we use as the systematic error. This error is taken as constant with redshift, since there is no clear dependence when the differences are plotted as a function of redshift (bottom panel).

5.4.5 Other systematic errors

There are some other potential systematic errors, like those arising from the uncertainty in the description of the redshift space distortions, the gravitational lensing magnification or those mainly associated with the used galaxy sample, as the bias of the population.

The uncertainties in the description of the redshift space distortions can induce a systematic error in the determination of the sound horizon scale. To evaluate it, we have changed the parameters of the z-distortions within their uncertainties, finding a value of $\Delta\theta_{\mathrm{BAO}} \sim 0.5$–1 per cent, in good agreement with the effect seen in Fig. 5.

At the BAO scales it is a good approximation to consider that the bias is scale independent (Cresswell & Percival 2009; Crocce et al. 2010b), and given the width of the redshift bins, we can safely use a redshift-independent bias inside each bin. The redshift dependence of bias may appear in a different normalization of the correlation function between different redshift bins. Since we do not care for the overall normalization but only about the position of the peak, we are not sensitive to $b(z)$. We have tested that the change in the overall amplitude of the correlation function does not affect our determination of the sound horizon scale, even if the error in the correlation function is changed. Moreover, we have tested the effect of a scale-dependent bias, introducing artificially the effect in the correlation functions, using an approximated Q-model with the determination of parameters of Cresswell & Percival (2009). The bias variation with θ in the fit region of $\omega(\theta)$ ranges from 1 to 6 per cent and induces a change in the determination of the sound horizon scale below 1 per cent, well within statistical uncertainties.

Finally, the gravitational lensing magnification can affect the $\omega(\theta)$ (Loverde et al. 2008) introducing correlations between bins at different redshifts. However, the effect of the magnification is concentrated at very low angles, and the magnitude of the induced correlation is much smaller than the correlation induced by photo-z, which has already been studied and used in this analysis. Therefore, the position of the BAO peak is free of systematics coming from magnification. Consequently, all this effect is not considered here.

6 CONCLUSIONS

We have developed a new method to measure the BAO scale in the angular two-point correlation function. This method is adapted to photometric redshift surveys, where the information along the line of sight is lost due to the photo-z precision, and only the angular information survives, although it can be applied to any survey. Two main results are found. First, the sound horizon scale can be recovered from the non-linear angular correlation functions to a precision of ≤ 0.75 per cent applying the parametric fit described in the text, for any cosmological model for infinitesimal redshift shells (i.e. for the 3D correlation function). This is not totally surprising. It can be understood if we approximate the 3D linear correlation as a sum of a BAO Gaussian and a baseline that is well described by a power law. If we neglect mode coupling effects, then the non-linear correlation will be given by a convolution with a Gaussian damping, which leaves unchanged the Gaussian position. Under this assumption, our parametric fit should be able to recover the true BAO positions without any bias. Secondly, the shift of the BAO peak due to projection effects has a universal shape, does not depend on the cosmological model and only depends on the redshift and the redshift bin width. This can be used to correct the result obtained for wide photo-z bins and recover the true sound horizon scale. The method has been tested with a mock catalogue built upon a large

N-body simulation provided by the MICE collaboration, with characteristics similar to those expected in DES. The true cosmology is recovered within 1σ. The correlation between redshift bins and a preliminary evaluation of the systematic errors has been included in this study, and we find that the most important systematic error arises from the photo-z precision. The method is very promising and very robust against systematic uncertainties.

Note that our analysis over the MICE simulations was in real, rather than in redshift, space; over a comoving output, rather than over an evolving distribution; and over dark matter particles, instead of galaxies. We believe that all these simplifications are not essential limitations to the method presented here, as we have shown that both the modelling and the error analysis are quite generic and work in real, redshift and photo-z space. If anything, redshift space distortions (and possibly biasing) produce larger amplitudes, in which case our results are conservative in the sense that more realistic simulations (or observations) will produce smaller error bars than the ones presented here.

REFERENCES

Banerji M., Abdalla F. B., Lahav O., Lin H., 2008, MNRAS, 386, 1219
Benítez N. et al., 2009, ApJ, 691, 241
Benjamin J., Van Waerbeke L., Menard B., Kilbinger M., 2010, MNRAS, 408, 1168
Bharadwaj S., 1996, ApJ, 472, 1
Cabre A., Fosalba P., Gaztanaga E., Manera M., 2007, MNRAS, 381, 1347
Colless M. et al., 2001, MNRAS, 328, 1039
Cresswell J. G., Percival W. J., 2009, MNRAS, 392, 682
Crocce M., Scoccimarro R., 2006, Phys. Rev. D, 73, 063519
Crocce M., Scoccimarro R., 2008, Phys. Rev. D, 77, 023533
Crocce M., Fosalba P., Castander F. J., Gaztanaga E., 2010a, MNRAS, 403, 1353
Crocce M., Cabré A., Gaztañaga E., 2010b, MNRAS, submitted (arXiv:1004.4640)
Eisenstein D. J. et al., 2005, ApJ, 633, 560
Eisenstein D. J., Seo H., White M., 2007, ApJ, 664, 660
Fisher K. B., Lahav O., Hoffman Y., Lynden-Bell D., Zaroubi S., 1995, MNRAS, 272, 885
Fosalba P., Gaztañaga E., Castander F. J., Manera M., 2008, MNRAS, 391, 435
Gaztañaga E., Cabré A., Hui L., 2009, MNRAS, 399, 1663
Hütsi G., 2006a, A&A, 449, 891
Hütsi G., 2006b, A&A, 459, 375
Ilbert O. et al., 2006, A&A, 457, 841
Kaiser N., Tonry J. L., Luppino G. A., 2000, PASP, 112, 768
Komatsu E. et al., 2010, ApJ, submitted (arXiv:1001.4538)

Landy S. D., Szalay A. S., 1993, ApJ, 412, 64

Loverde M., Hui L., Gaztañaga E., 2008, Phys. Rev. D, 77, 023512

Matsubara T., 2008, Phys. Rev. D, 77, 063530

Matsubara T., Szalay A. S., Pope A. C., 2004, ApJ, 606, 1

Nock K., Percival W. J., Ross A. J., 2010, MNRAS, 407, 520

Okumura T., Matsubara T., Eisenstein D. J., Kayo I., Hikage C., Szalay A. S., Schneider D. P., 2008, ApJ, 676, 889

Padmanabhan N., White M., 2009, Phys. Rev. D, 80, 063508

Padmanabhan N. et al., 2007, MNRAS, 378, 852

Peebles P. J. E., 1980, The Large-Scale Structure of the Universe. Princeton Univ. Press, Princeton, NJ

Percival W. J., Cole S., Eisenstein D. J., Nichol R. C., Peacock J. A., Pope A. C., Szalay A. S., 2007, MNRAS, 381, 1053

Rassat A. et al., 2008, preprint (arXiv:0810.0003)

Sánchez A. G., Baugh C. M., Angulo R., 2008, MNRAS, 390, 1470

Sánchez A. G., Crocce M., Cabré A., Baugh C. M., Gaztañaga E., 2009, MNRAS, 400, 1643

Seo H., Eisenstein D. J., 2007, ApJ, 665, 14

Seo H., Siegel E. R., Eisenstein D. J., White M., 2008, ApJ, 686, 13

Seo H. et al., 2010, ApJ, 720, 1650

Simpson F., Peacock J. A., Simon P., 2009, Phys. Rev. D, 79, 063508

Smith R. E., Scoccimarro R., Sheth R. K., 2008, Phys. Rev. D, 77, 043525

The Dark Energy Survey Collaboration, 2005, preprint (astro-ph/0510346)

Tyson J. A., Wittman D. M., Hennawi J. F., Spergel D. N., 2003, Nuclear Phys. B Proc. Suppl., 124, 21

York D. G. et al., 2000, AJ, 120, 1579

This paper has been typeset from a T$_{\rm E}$X/L$^{\rm A}$T$_{\rm E}$X file prepared by the author.